A REDUCED ORDER MODEL FOR DYNAMIC LOADS PREDICTION INCLUDING AERODYNAMIC NONLINEARITIES

David Quero[1], Wolf Krüger[1] and Guillermo Jenaro[2]

[1]DLR (German Aerospace Center), Göttingen, Germany

[2]Airbus Operations GmbH, Hamburg, Germany

Keywords: ROM, AIC correction, gust encounter, dynamic loads

Abstract: In this paper a novel frequency domain Reduced Order Model (ROM) to compute the dynamic response to atmospheric disturbances of a free aircraft flying in the transonic regime including CFD aerodynamics is presented. It is based on correction of the unsteady Aerodynamic Influence Coefficient (AIC) matrices. First, the ROM is applied within the aerodynamic linear region where effects can be superposed using a minimum number of unsteady CFD computations and validated against results obtained by direct coupled CFD-CSM simulation. Additionally, the ROM is extended into a nonlinear region linearizing around a dynamic state instead of the usual steady state linearization. Again, results are validated against direct coupled nonlinear time domain simulations.

NOMENCLATURE

f, ω, k	Frequency, circular frequency and reduced frequency
L_{ref}	Reference length, half of the Mean Aerodynamic Chord (MAC)
q, U_∞	Dynamic pressure and freestream velocity
$\mathbf{Q}$, $\mathbf{Q_c}$	AIC matrixand corrected AIC matrix at a particular reduced frequency
$\triangle\mathbf{Q}$	Incremental AIC matrix,
$\mathbf{w}$	Downwash matrix
$\triangle\mathbf{c_p}$	Incremental (between upper and lower surface) pressure coefficient distribution
$\mathbf{A}$	Left hand side matrix in the frequency domain least squares problem
$\widetilde{\mathbf{x}}$	Solution vector to the frequency domain least squares problem
$\mathbf{b}$	Righ hand side vector in the frequency domain least squares problem
$\mathbf{P}$	Matrix containing the CFD predicted quantities
$\mathbf{P}_0$	Matrix containing the DLM predicted quantities
$\mathbf{x_0}$	Vector with normalized elements of the original AIC matrix
$\widetilde{\mathbf{A}}$	Matrix to obtain quantites from incremental pressure coefficient distribution
N, N_r	Total number of DLM panels, subset of panels used for correction
N_c, N_s, M	Number of constraints, aerodynamic strips and correction modes
$\mathbf{L}$, $\mathbf{M}$	Matrix to compute local lift and local pitch moment coefficients
C_{li}, C_{mi}	Lift and pitch moment coefficient of aerodynamic strip i
$\Phi_{g\eta}$	Modal matrix to transform from physical dof to modal dof
H_{kg}	Spline matrix to spline displacements from structural grid to aerodynamic grid
S_{kj}	Summation matrix from pressure coefficient to force and moment
$GAF_{\eta m}$	Generalized Aerodynamic Force, correction mode m and vibration mode η
F_{im}	Total aerodynamic load at structural node g, dof i
w_ε	Downwash tolerance
$w\,(x,t)$	Vertical velocity imposed at coordinate x and instant t

w_0	Gust amplitude
L_g, H	Gust length, gust gradient (half of the gust length)
x_0, t_0	Gust initial position and time
$\eta\,(t)$	Generalized coordinate time history
t_{max}	Exponential pulse duration
$\mathbf{D}_{1jk}$, $\mathbf{D}_{2jk}$	Substantial derivative matrices
$\mathbf{M}_{\eta\eta}$	Generalized mass matrix
$\mathbf{B}_{\eta\eta}$	Generalized damping matrix
$\mathbf{K}_{\eta\eta}$	Generalized stiffness matrix
$\mathbf{Q}_{\eta\eta}$	Generalized AIC matrix

1 INTRODUCTION

Dynamic loads due to atmospheric disturbances are of capital importance when designing and sizing an aircraft. There are very well established linear methods to compute the aerodynamic loads, both in frequency and time domain, which properly represents the physics for subsonic cases, where the aerodynamic remains linear. Probably the best kown is the Doublet-Lattice Method (DLM) in frequency domain, which solves the unsteady compressible potential equation.

In this work the nonlinearities refer to the aerodynamic contribution. In the transonic regime, where nonlinear aerodynamic effects such as recompression shocks, viscosity and separation become important, the classical methods differ from reality and additional conservatism is considered in the design. High fidelity methods, which are able to better capture the aerodynamic nonlinear effects involved in the transonic regime, are key in order to potentially reduce this conservatism. However, high fidelity methods cannot be used as such in a realistic design process, where thousands of cases must be considered. Thus, processes allowing the robustness and efficiency of the classical methods but including a better physical description of the phenomena involved in the transonic regime are sought. This kind of approach is referred to as model reduction.

In this paper a novel ROM to compute the dynamic response of a free aircraft to an atmospheric disturbance is presented. The focus is on the free response to a discrete gust, in particular vertical gusts of the form 1-cos, but can be applied to any kind of external perturbation, such as gust, turbulence or wake vortex encounter.

The topic has been adressed by several authors. Two different approaches are available for model reduction, both applicable in time and frequency domain.

One approach includes the projection methods, where the full model is manipulated to reduce the overall computational cost. An application to gust computations has been done by Da Ronch [1]. There, cases for discrete and continuous gust of small amplitudes over a rigid profile and a cantilevered wing are considered. Timme [2] applies it to a flexible aircraft, showing the limitation of the method for realistic configurations. A Proper Orthogonal Decomposition (POD) method combined with a convolution scheme is generated for a Truss Braced Wing (TBW) aircraft by Bartels [3]. *Rigid* gust (aircraft motion is not allowed) results for moderate gust amplitudes (up to 4% of the freestream

velocity) are shown. Wales [4] presents an Eigensystem Realisation Algorithm (ERA) ROM for a rigid wing including some nonlinear effects from steady computations.

The other approach is referred to as sytem identification methods, where a low order model is developed based on known responses to particular inputs. A time domain based Auto Regressive-Moving-Average (ARMA) model and a Generalized Aerodynamic Force (GAF) convolution based frequency domain ROM are presented by Raveh [5]. An application to a bidimensional case for gust cases is done by Zaide and Raveh [6] and by Raveh [7] for a rigid wing. Application to a free elastic aircraft is done by Raveh [8]. There the ROM application cases are focused on the linear aerodynamic region, where the different aerodynamic effects can be superposed. Results within the aerodynamic nonlinear region are presented by Raveh [9], where the limitation of the ROM is pointed out. A method based on a Taylor expansion around frequency zero for a diagonal modification of the AIC matrices, as proposed by Chen [10] and extended by Thormann [11], is applied to gust encounters by Dimitrov [12]. There, results of several gust profiles over a rigid wing are shown. The method is valid for cases where the main difference with respect to higher fidelity results are caused by an offset difference in magnitude and not in phase in frequency domain, thus limiting the method to very small gust amplitudes.

In the current work a system identification ROM method is developed in frequency domain which tries to overcome limitations present in other methods. It is based on the modification of the unsteady AIC matrices, allowing the identification of the system for some particular correction modes and its extension to different modes. This ROM aims to match not only the aircraft response but also the loads distribution as provided by higher fidelity methods, and using a number of CFD unsteady computations lower than the total number of external perturbation and vibration modes. It uses CFD data obtained in time domain, and thus aerodynamic effects as resonance peaks in frequency domain can be reproduced, provided they are included in the frequency domain description of the reference computations. Additionally, the correction modes used as reference may have a physical meaning, being easier to identify the driving modes for particular cases.

2 LEAST SQUARES IN FREQUENCY DOMAIN

2.1 Optimization problem

As it has been stated, the ROM is based on the modification of the AIC matrices in frequency domain. Thus a Doublet-Lattice grid and a set of AIC matrices are assumed to be available. In the present work they are computed by the commercial software MSCNastran. Additionally, the required unsteady CFD computations are assumed to be available in time domain.

The Mach number for the DLM reference model and the CFD computations is set to be the same. Additionally, the initial steady angle of attack for the CFD computations is fixed, but different values can be easily considered. The CFD data provides the reference data to be matched by the modified (or corrected) AIC, and it is defined by a set of input correction modes together with the corresponding time domain results. One or several correction modes can be considered simultaneously, and any flow disturbance, such as a gust profile, a structural motion, or a combination is allowed. For the ROM generation, a correction mode is defined by its downwash distribution over the Doublet-Lattice panels,

being the downwash the local disturbance velocity perpendicular to the panel, as imposed by the no-penetration boundary condition. For a particular correction mode, the position and grid velocity over the cells on the CFD surface grid (needed for the time domain CFD computation) together with the downwash distribution (needed for the modified AIC generation) are required.

Now the problem is stated. The AIC matrices are to be modified so that the CFD time domain reference results when applying the corresponding downwash over the Doublet-Lattice grid, comprising N panels. This can be expressed as shown in Eq. 1 for each frequency value, where $\mathbf{Q_c}$ denotes the corrected AIC matrix, $\mathbf{w}$ the dimensionless (with the freestream velocity U_∞) downwash distribution vector and $\triangle\mathbf{c_p}$ the incremental (difference between lower and upper panel surface) pressure coefficient, as obtained from CFD. It is usual to specify the frequency f (Hz) in a dimensionless reduced frequency k as specified in Eq. 2, where L_{ref} is the reference longitude (usually half of the mean aerodynamic chord value). Premultiplying by a matrix $\widetilde{\mathbf{A}}$ Eq. 1 can be written in more general terms as Eq. 3, see Eq. 4. By doing so, a number N_c of different quantities other than the pressure coefficient may be considered, such as local aerodynamic coefficients, nodal load, etc. Note that an additional scheme is required in order to interpolate the incremental pressure coefficient from the CFD surface grid into the Doublet-Lattice grid, see Thormann [11]. In Eq. 1 a number M of downwash and incremental pressure coefficient distributions can be considered (correction modes), provided they are specified in different columns in the matrices $\mathbf{w}$ and $\mathbf{P}$, see Eq. 5 and 6, where w_{mp} is the downwash over panel p for mode m, being $p = 1, ..., N$ and $m = 1, ..., M$. In general, the vector containing the values to be matched $\mathbf{P}$ can be obtained by experimental or computational methods. In this work computational values obtained from CFD time simulations are imposed.

$$\mathbf{Q_c w} = \triangle\mathbf{c_p} \tag{1}$$

$$k = \frac{2\pi f L_{ref}}{U_\infty} \tag{2}$$

$$\widetilde{\mathbf{A}}\mathbf{Q_c w} = \mathbf{P} \tag{3}$$

$$\mathbf{P} = \widetilde{\mathbf{A}}\triangle\mathbf{c_p} \tag{4}$$

$$\mathbf{w} = \begin{bmatrix} w_{11} & ... & w_{m1} & ... & w_{M1} \\ ... & ... & ... & ... & ... \\ w_{1p} & ... & w_{mp} & ... & w_{Mp} \\ ... & ... & ... & ... & ... \\ w_{1N} & ... & w_{mN} & ... & w_{MN} \end{bmatrix}_{N\times M} \tag{5}$$

$$vec\left(\mathbf{P}\right) = \begin{bmatrix} \mathbf{P}_1 \\ \cdots \\ \mathbf{P}_m \\ \cdots \\ \mathbf{P}_M \end{bmatrix}_{(N_c \cdot M)\times 1} \tag{6}$$

There are $N \cdot M$ known values (or equations) and N^2 unknowns (the corrected matrix $\mathbf{Q_c}$ is a full matrix). In practical cases there are less than N number of CFD computations available and thus there are more unknowns than equations. This leads to the solution of an underdetermined problem. This means there is an infinite number of solutions satisfying Eq. 1, from which a minimum norm solution can be chosen in order to specifiy an unique one. In general, the data over all panels do not need to be available, but only for a number of panels $N_r \leq N$, resulting in the modification of the rows corresponding only to this subset of panels in $\mathbf{Q_c}$. However, the downwash distribution must be specified over all panels, being the number of unknowns $N_r \cdot N$. The minimum norm solution $\widetilde{\mathbf{x}}$ of the optimization problem defined by Eq. 7 and 8 is sought.

$$min\left(\sum_{i=0}^{i=N_r \cdot N} \left\|\tilde{\mathbf{x}}\right\|^2\right) \tag{7}$$

$$\mathbf{A}\tilde{\mathbf{x}} = \mathbf{b} \tag{8}$$

The problem defined in Eq. 1 must now be rewritten in the form specified by Eq. 8. In order to do so, the Kronecker product $\otimes$ and the *vec* operator as defined in Henderson [13] are used, see 9. The unknown vector $\tilde{\mathbf{x}} = vec\left(\mathbf{x}\right)$ does not include directly the elements of $\mathbf{Q_c}$ but has been redefined instead, see Eq. 10, where $\triangle\mathbf{Q}$ denotes the additional corrected AIC matrix as shown in Eq. 11, $\mathbf{Q_c}$ the modified AIC and $\mathbf{Q}$ the original one. Note that the dependency with the reduced frequency k has been explicitely pointed out in Eq. 10. Using this definition of the unknown vector, the corrected matrix $\mathbf{Q_c}$ at this particular frequency is in a least squares sense the closest possible (in magnitude) to the original AIC matrix $\mathbf{Q}$ and AIC elements with a higher magnitude value are stronger modified. Additionally, the quantity values as predicted by the original $\mathbf{Q}$ must be substracted in the right hand side, see Eq. 12, 13 and 14.

$$\left(\mathbf{w}^T \otimes \widetilde{\mathbf{A}}\right) vec\left(\mathbf{x}\right) = \mathbf{b} \tag{9}$$

$$\begin{aligned} vec(\mathbf{x}) \;=\; [\; & \frac{\triangle Q_{11}(k)}{\sqrt{|Q_{11}(k)|}} \;\; \cdots \;\; \frac{\triangle Q_{N_r 1}(k)}{\sqrt{|Q_{N_r 1}(k)|}} \;\; \frac{\triangle Q_{12}(k)}{\sqrt{|Q_{12}(k)|}} \;\; \cdots \\ & \frac{\triangle Q_{N_r 2}(k)}{\sqrt{|Q_{N_r 2}(k)|}} \;\; \cdots \;\; \frac{\triangle Q_{1N_p}(k)}{\sqrt{\left|Q_{1N_p}(k)\right|}} \;\; \cdots \;\; \frac{\triangle Q_{N_r N_p}(k)}{\sqrt{\left|Q_{N_r N_p}(k)\right|}} \;]^T_{(N_r \cdot N)\times 1} \end{aligned} \tag{10}$$

$$\mathbf{Q_c} = \mathbf{Q} + \triangle\mathbf{Q} \tag{11}$$

$$\mathbf{b} = vec\left(\mathbf{P}\right) - vec\left(\mathbf{P}_0\right) \tag{12}$$

$$vec\left(\mathbf{P}_0\right) = \left(\mathbf{w}^T \otimes \widetilde{\mathbf{A}}\right) vec\left(\mathbf{x_0}\right) \tag{13}$$

$$\begin{aligned} vec(\mathbf{x_0}) \;=\; [\; & \frac{Q_{11}(k)}{\sqrt{|Q_{11}(k)|}} \;\; \cdots \;\; \frac{Q_{N_r1}(k)}{\sqrt{|Q_{N_r1}(k)|}} \;\; \frac{Q_{12}(k)}{\sqrt{|Q_{12}(k)|}} \;\; \cdots \\ & \frac{Q_{N_r2}(k)}{\sqrt{|Q_{N_r2}(k)|}} \;\; \cdots \;\; \frac{Q_{1N_p}(k)}{\sqrt{\left|Q_{1N_p}(k)\right|}} \;\; \cdots \;\; \frac{Q_{N_rN_p}(k)}{\sqrt{\left|Q_{N_rN_p}(k)\right|}} \;]^T_{(N_r \cdot N)\times 1} \end{aligned} \tag{14}$$

Matrix dimensions are shown in Eq. 15, 16 and 17. In a general case the number of quantities or constraints $N_c \leq N_r \cdot N$ depends on the quantities chosen to be matched.

$$\mathbf{A} = \left(\mathbf{w}^T \otimes \widetilde{\mathbf{A}}\right)_{(N_c \cdot M)\times(N_r \cdot N)} \tag{15}$$

$$\widetilde{\mathbf{x}} = vec\left(\mathbf{x}\right)_{(N_r \cdot N)\times 1} \tag{16}$$

$$\mathbf{b} = vec\left(\mathbf{P}\right)_{(N_r \cdot N)\times 1} \tag{17}$$

Once the problem has been stated, the solution is equivalent to applying the Lagrange multiplier method to the constrained optimization problem, in which the vector $\widetilde{\mathbf{x}}$ subject to the equality constraint $\mathbf{Ax} = \mathbf{b}$ minimizes the (squared) norm $\|\widetilde{\mathbf{x}}^2\|$, see Eq. 18, whose solution is given in Eq. 19, see Yang [14]. Once the problem has been solved for $\hat{\mathbf{x}}$, its elements are rearranged and by means of Eq. 11 the corrected matrix $\mathbf{Q_c}$ is found.

$$Min(\tilde{\mathbf{x}}, \lambda) = \frac{1}{2}\left\|\tilde{\mathbf{x}}\right\|^2 - \boldsymbol{\lambda}^T\left(\mathbf{A}\tilde{\mathbf{x}} - \mathbf{b}\right) = \frac{1}{2}\tilde{\mathbf{x}}^T\tilde{\mathbf{x}} - \boldsymbol{\lambda}^T\left(\mathbf{A}\tilde{\mathbf{x}} - \mathbf{b}\right) \tag{18}$$

$$\tilde{\mathbf{x}} = \mathbf{A}^T\boldsymbol{\lambda} = \mathbf{A}^T\left[\mathbf{A}\mathbf{A}^T\right]^{-1}\mathbf{b} \tag{19}$$

This problem has been solved at frequency zero by Bruns and Brink-Sparlink [14]. It is also pointed out the possibility to apply the correction at particular frequencies higher than zero. In that case the matrices $\mathbf{A}$, $\mathbf{x}$ and $\mathbf{b}$ become in general complex and thus the Hermitian adjoint $\mathbf{A}'$ instead of the tranpose $\mathbf{A}^T$ is to be considered, see Miller [16].

The matrix $\widetilde{\mathbf{A}}$ will be specified now. This matrix contains the same submatrix $\widetilde{\mathbf{A}_m}$ for each correction mode repeated M times, see Eq. 20. In this work three different possibilities have been implemented.

$$\widetilde{\mathbf{A}} = \begin{bmatrix} \widetilde{\mathbf{A}_1} \\ ... \\ \widetilde{\mathbf{A}_m} \\ ... \\ \widetilde{\mathbf{A}_M} \end{bmatrix}_{(N_c \cdot M) \times N_r} \tag{20}$$

- Matrix $\widetilde{\mathbf{A}}$ to extract the local lift and pitch moment coefficient at different aerodynamic strips, see Eq. 21. It is assumed that the coefficients are known in frequency domain at a number N_s of aerodynamic strips. The number of constraints is $N_c = 2N_s$. In this case summation matrices $\mathbf{L}$ for lift coefficient computation and $\mathbf{M}$ for pitch moment computation are created. Their matrix elements L_{sp} and M_{sp} are given in Eq. 22 and 23, where $s = 1, ..., N_s$ and $p = 1, ..., N_r$.

$$\widetilde{\mathbf{A}_m} = \begin{bmatrix} \mathbf{L} \\ \mathbf{M} \end{bmatrix}_{N_c \times N_r} \tag{21}$$

$$L_{sp} = \begin{cases} A_p, & \text{if the panel belongs to this strip, } p \epsilon s, \\ 0, & \text{otherwise.} \end{cases} \tag{22}$$

$$M_{sp} = \begin{cases} A_p \left[\begin{bmatrix} x_p - x_{(c/4)s} & 0 & 0 \end{bmatrix}^T \times \mathbf{n}_p \right] \cdot \left[\begin{bmatrix} 1 & 0 & 0 \end{bmatrix}^T \times \mathbf{n}_p \right], & \text{if } p \epsilon s, \\ 0, & \text{otherwise.} \end{cases} \tag{23}$$

, where A_p is the area of the panel p, x_p its x coordinate and $\mathbf{n_p}$ its normal vector. The coordinate $x_{(c/4)s}$ represents the $c/4$ chord point of the strip s, which is the convention adopted for the local moment. The pitch moment is positive if produces a nose up moment over the strip. In this case $vec\,(\mathbf{P})$ is given in Eq. 24.

$$vec\,(\mathbf{P}) = \begin{bmatrix} C_{l1} & ... & C_{li} & ... & C_{ls} & C_{m1} & ... & C_{mi} & ... & C_{ms} \end{bmatrix}^T_{2N_s \times 1} \tag{24}$$

, being C_{li} and C_{mi} the local lift and local pitch moment coefficient at the strip $i = 1, ..., N_s$.

- Matrix $\widetilde{A}$ to extract the GAF (Generalized Aerodynamic Forces). In this case additional matrices to build $\widetilde{\mathbf{A}}$ are required, which is given by Eq. 25, where $\boldsymbol{\phi}_{g\eta}$ is the modal matrix including the specific subset η of modal coordinates to be matched, $\mathbf{H}_{kg}$ is the spline matrix which transfers structural displacements to aerodynamic displacements (its transpose transfers aerodynamic loads to structural loads) and $\mathbf{S}_{kj}$ is the summation matrix which converts pressure distribution over the subset of panels to nodal forces and moments. The $vec\,(\mathbf{P})$ term is obtained taking the vec operator to the element $GAF_{\eta m}$. The number of constraints is then $N_c = \theta \cdot M$, where $\eta = 1, ..., \theta$, being θ the number of modal coordinates chosen to be matched.

$$\widetilde{\mathbf{A}} = \boldsymbol{\phi}^T_{g\eta} \mathbf{H}^T_{kg} \mathbf{S}_{kj} \tag{25}$$

- Matrix $\widetilde{A}$ to extract the nodal loads due to the aerodynamic effects, that is, due to the external air perturbation and the aircraft motion, see Eq. 26. The nodal force (due to aerodynamic effects) at the structural node for the correction mode m is denoted by F_{xim}, F_{yim} and F_{zim} for the nodal force in the x, y and z directions respectively, where $i = 1, ..., N_G$, being N_G the total number of structural nodes. The number of constraints is $N_c = 3N_G \cdot M$. Again, a subset among all structural nodes can be selected. Also, the force along only some direction can be matched.

$$\widetilde{\mathbf{A}} = \mathbf{H}_{kg}^{T}\mathbf{S}_{kj} \tag{26}$$

These three possibilities can be combined and quantities involving local aerodynamic coefficients, GAF and aerodynamic nodal loads can be matched simultaneously.

2.2 Numerical implementation

As stated above, a correction mode may be defined by a gust profile of a specific length (or frequency), a vibration mode, a synthetic mode describing a particular structural motion or a combination of those. However the correction modes must be linearly independent in order for the LSQ problem not to become singular.

The reference values to be matched are obtained after applying the Fast Fourier Transform (FFT) transformation as defined in Eq. 27 to each of the quantity time histories obtained by CFD. The discrete signal in time is defined by the y_j values in the time interval $[0, N\triangle t]$. With the time signal y sampled with a constant time interval $\triangle t$ its frequency domain representation is given by the signal Y_k in the frequency interval $[0, 1/2\triangle t]$ (Hz). For a more detailed description see Karpel [17].

$$Y_k = \triangle t \sum_{j=0}^{N-1} y_j e^{-i2\pi jk/N}, \quad k = 0, ..., N-1 \tag{27}$$

The FFT values of the quantities chosen to be matched (see Eq. 24) form the right hand side of the LSQ problem at each reduced frequency, see Eq. 6.

For all quantities in $\mathbf{P}$ from different correction modes to have the same frequency domain discretization, the signals in time domain are interpolated to a common time discretization with proper time step and time end values.

In order to generate numerically stable corrected AIC matrices, the problem defined by Eq. 7 cannot be solved for all correction modes at every reduced frequency. If for a particular correction mode a specific reduced frequency is practically not excited, this mode is excluded from the LSQ problem. A correction mode m is included in the LSQ problem at a reduced frequency k if the condition defined in Eq. 28 is fulfilled, where $\mathbf{w_m}(k)$ is the downwash distribution corresponding to mode m and k^* denotes all reduced frequency values smaller than the particular one under consideration. Note that now the dependency with the reduced frequency has been explicitly pointed out. The first k value at which the mode m does not fulfill this condition is the maximum allowed reduced frequency for that mode. In general each correction mode possesses a different maximum allowed reduced frequency. The tolerance value has been set in this work to $w_\varepsilon = 10^{-3}$.

$$\frac{max\left(|\mathbf{w}_m\left(k\right)|\right)}{max\left(|\mathbf{w}\left(k^* \leq k\right)|\right)} \geq w_\epsilon, \quad m = 1, ..., M \tag{28}$$

The LSQ problem is solved at each reduced frequency k with QR decomposition of the matrix $\mathbf{A}$.

2.3 Methodology

The presented ROM allows a subset of quantities to be matched. For example, only the aerodynamic strips belonging to a certain component may be corrected, keeping the aerodynamic description of other components as predicted by the original DLM. Also, being the modified AIC matrix full, interference effects can be included.

2.3.1 CFD

The CFD results are obtained with the TAU-Code [18]. For the flux discretization a central scheme is used. The temporal discretization includes a local time stepping scheme for steady calculations and a dual time stepping algorithm for unsteady computations. Results obtained for an Euler grid are shown in the present work. In order to model the gust effect, the Field Velocity Method (FVM) is implemented, where the gust velocity is prescribed at every grid node and the effect of the aircraft on the gust is neglected [19,20]. The Split Velocity Method (SVM) includes this effect, see Wales [21], who has developed it for the Euler equations and where it is shown that the use of the FVM is justified for practical cases.

In order to demonstrate the ROM unsteady capabilities, the influence of the steady trim has been neglected in the coupled CFD-CSM computation. Thus, the initial dynamic shape of the model does not include static deformation and only incremental unsteady forces are considered for the aircraft response. The generalized coordinates are set to zero at the beginning of the simulation and only the incremental dynamic response is considered.

2.3.2 Corrected AIC generation

As already stated, a Doublet-Lattice grid together with AIC matrices is required for the corrected AIC matrices generation. They are assumed to be available.

In this work both a quasi-steady and a full unsteady correction are considered. The quasi-steady correction has been implemented as done in [12]. In this case the corrected AIC matrix at any reduced frequency is computed as function of the corrected and original AIC matrix at frequency zero, see Eq. 29. This quasi-steady correction is referred to as an offset correction, as a shift is applied to the real part of the AIC matrix elements. The full unsteady correction is applied as described in section 2.2. The vector $vec\left(\mathbf{P}\right)$ in Eq. 12 contains the finite difference values generated by two steady computations, one corresponding to the initial steady angle of attack and the other setting the angle of attack to the steady value plus an incremental value of 0.1 (deg).

$$\mathbf{Q_c}(k) = \mathbf{Q}(k) + \mathbf{Q_c}(k = 0) - \mathbf{Q}(k = 0) \tag{29}$$

Results obtained with the matrix $\widetilde{\mathbf{A}}$ as given in Eq. 21 are shown. For this case there is no need of mapping the complete pressure coefficient surface field over the Doublet-Lattice panels. Instead, the local aerodynamic coefficients are computed at each strip from the CFD surface pressure values. Thus the matrix $\widetilde{\mathbf{A}}$ is not used in Eq. 4, being the $\mathbf{P}$ values computed directly from the available CFD results. In order to avoid numerical instability, the integration has been carried out over the initial undeformed mesh but considering the current pressure values. Once the time histories of the aerodynamic coefficients are available for the strips of interest, their values are converted into frequency domain using Eq. 27 for each aerodynamic strip coefficient. When focusing on vertical discrete gusts, the aerodynamic strips belonging to the wing and horizontal tail plane are considered, neglecting the vertical tail plane.

For the full unsteady correction, in order to generate the time domain CFD results corresponding to the correction modes the input to the computation has to be defined. It is known that for Linear Time Invariant (LTI) systems the transfer functions which describe their behavior in frequency domain do not depend on the input signal. It is then sufficient to excite the system with an input signal and compute the transfer function once the output is known. The ideal input is the impulse, which in theory excites all frequencies. As we are dealing with discrete systems though, the impulse is approximated by a discrete pulse signal. For numerical stability a smooth signal is preferred rather than a discrete value acting at an unique time value. The shorter the pulse, the wider the frequency spectrum excited. Note that the pulse shape does not modify the system properties, provided the reduced frequency range of interest is excited by the input.

Three types of pulse input shapes are used.

- $(1 - cos)$ pulse. This shape is used when the correction mode is a discrete gust profile. In this case the velocity field (over surface panels for the LSQ problem and over the cells grid in CFD) is specified as given in Eq. 30, where w_0 is the pulse amplitude, L_g the pulse length and $t^*(x)$ as given in Eq. 31 stands for the penetration effect caused by the gust translating at velocity U_∞, being t_0 and x_0 respectively an initial time and distance (in x direction) offsets between the gust and the aircraft nose. The pulse reduced frequency k_g is defined by its length L_g or gradient H, defined to be the half of its length, $L_g = 2H$, and given in Eq. 32.

$$w(x,t) = \begin{cases} \frac{w_0}{2}\left(1 - cos\frac{2\pi U_\infty (t - t^*(x))}{L_g}\right), & t^*(x) \leq t \leq t^*(x) + \frac{L_g}{U_\infty}, \\ 0, & else \end{cases} \tag{30}$$

$$t^*(x) = t_0 + \frac{(x - x_0)}{U_\infty} \tag{31}$$

$$k_g = \pi\left(\frac{L_{ref}}{H}\right) \tag{32}$$

- Exponential shape of duration t_{max} as used by Marques [22]. In this case the time histoy of a generalized coordinate η is specified as given in Eq. 33.

$$\eta(t) = \begin{cases} 4\left(\frac{t}{t_{max}}\right)^2 \exp\left(2 - \frac{1}{1-\frac{t}{t_{max}}}\right), & 0 \leq t \leq t_{max}, \\ 0, & t \geq t_{max} \end{cases} \tag{33}$$

- General shape. Used when the correction mode is a combination of a gust and a general structural motion, which can be a combination of predefined time histories in the generalized coordinates. This type of input shape is only used when generating the ROM in the nonlinear aerodynamic region.

2.3.3 Linear aerodynamic region

In this region the aerodynamic effects may be superposed. This is justified when considering small gust amplitudes. Actually the boundary between the linear and nonlinear aerodynamic region is a combination of gust amplitude and frequency [23]. In order to decrease the time spent for the ROM generation, a minimum number of CFD computations is convenient. Additionally, the time for the generation of the corrected AIC increases with the number of correction modes taken into account. The ROM performance is analyzed by adding correction modes systematically. In particular, two cases are considered.

1. ROM including one correction mode, a high frequency gust in order to produce a wide range of reduced frequency available as provided by Eq. 28. For flutter-free aeroelastic applications is enough to consider the gust frequency corresponding to the shortest gust specified by the regulations, $H_{min} = 50$ (ft). In this case only one CFD computation is required, the corresponding to the velocity field specified by Eq. 30 with $L_g = 2H_{min}$. It is expected that the gust correction mode is able to represent the heave and pitch aerodynamic properties at low frequency, as their downwash distributions tend to the same one at zero frequency for an equivalent amplitude.
2. ROM including two correction modes, adding the first flexible mode (usually the first wing bending). Now an additional CFD computation is carried out by imposing the time history from Eq. 33 in the generalized coordinate corresponding to the first flexible mode.

Note that in the proposed method there is no need to run a CFD computation for each vibration mode and rigid body mode, as the frequency properties included in the corrected AIC are transferred between modes by means of the downwash vector. This allows for the number of CFD computations to be drastically reduced, usually at least in an order of magintude.

2.3.4 Nonlinear aerodynamic region

In this region the aerodynamic effects due to gust and structural motion may not be superposed as for example in the case of a particular combination of high amplitude and low frequency gust. The exact boundary as a combination of gust amplitude and frequency values depends on the particular case and is not the focus on this work. Both aerodynamic effects, due to the gust and the structural motion, are to be considered simultaneously. A direct coupled CFD-CSM simulation can provide the complete solution. However, the aim of the ROM in the nonlinear region is to provide a feasible description without having to run the CFD-CSM each time. A previous work can be found in [23].

Note that even though the problem in time domain is nonlinear, a frequency domain description of the problem as shown in Eq. 34 is possible by defining a set of modified AIC matrix is defined in $vec\,(\mathbf{x})$ (see Eq. 10) such that the nonlinear aerodynamics as predicted by the CFD-CSM computation is matched.

A constant frequency domain description is considered within the linear aerodynamic region by linearizing around the nonlinear steady state. Unlike for the linear region, in the nonlinear region the frequency domain description depends on the system input, defined by the gust and the aircraft response, which is unknown unless the direct coupled problem is solved. Instead, the frequency domain description is approximated by assuming the aircraft response to be as predicted by the DLM, which is equivalent to linearizing the problem around a given trajectory by assuming the aircraft response. The same idea is applied in the theory of describing functions for nonlinear control design, see [24], where a nonlinear system is *quasi*-linearized by assuming the input shape to the nonlinearity. In other words, the problem defined by Eq. 34 is aproximated by Eq. 35. The downwash matrix $\hat{\mathbf{w}}$ in Eq. 35 includes two correction modes.

1. Downwash vector $\hat{\mathbf{w}}_\mathbf{1}$=$\mathbf{w_g} + \mathbf{w_1}$ resulting from the superposition of the particular gust of interest with downwash vector $\mathbf{w_g}$ and the structural motion as predicted by DLM with downwash vector $\mathbf{w_1}$, given in Eq. 36, 37 and 38 in frequency domain. Note that the generation of $\mathbf{w_1}$ is computationally very cheap. Note that the (nonlinear) interaction between the gust and the structural motion is considered by the CFD results corresponding to this mode.
2. Downwash vector $\hat{\mathbf{w}}_\mathbf{2}$ due to a *linear* gust (by linear gust an amplitude and frequency combination within the aerodynamic linear region is meant). The shortest gust gradient H_{min} is considered in order to get a wider reduced frequency range.

$$\left(\mathbf{w}^T \otimes \widetilde{\mathbf{A}}\right) vec\,(\mathbf{x}) = \mathbf{vec}\,(\mathbf{P}) - \mathbf{vec}\,(\mathbf{P_0}) \tag{34}$$

$$\left(\hat{\mathbf{w}}^T \otimes \widetilde{\mathbf{A}}\right) vec\,(\hat{\mathbf{x}}) = \mathbf{vec}\left(\hat{\mathbf{P}}\right) - \mathbf{vec}\,(\mathbf{P_0}) \tag{35}$$

$$\mathbf{w_1} = (\mathbf{D}_{1jk} + ik\mathbf{D_{2jk}}) \left[-\omega^2\mathbf{M}_{\eta\eta} + i\omega\mathbf{B}_{\eta\eta} + \mathbf{K}_{\eta\eta} - q\mathbf{Q}_{\eta\eta}\,(k)\right]^{-1} q\mathbf{Q}_{\eta j}\,(k)\,\mathbf{w}_g \tag{36}$$

$$\mathbf{Q}_{\eta j}\,(k) = \boldsymbol{\phi}_{g\eta}^T \mathbf{H}_{kg}^T \mathbf{S}_{kj} \mathbf{Q}\,(k) \tag{37}$$

$$\mathbf{Q}_{\eta\eta}\,(k) = \mathbf{Q}_{\eta j}\,(k)\,(\mathbf{D}_{1jk} + ik\mathbf{D}_{2jk})\,\mathbf{H}_{kg}\boldsymbol{\phi}_{g\eta} \tag{38}$$

These two correction modes are included in $\hat{\mathbf{w}}$ and their corresponding aerodynamic strip coefficients in frequency domain as provided by the time domain CFD computations are included in $\mathbf{P}$. Then the LSQ problem defined in Eq. 35 is solved for $\hat{\mathbf{x}}$, which provides an approximation to the frequency domain representation of the direct coupled nonlinear CFD-CSM problem. After rearranging terms and using Eq. 11 a corrected AIC is found.

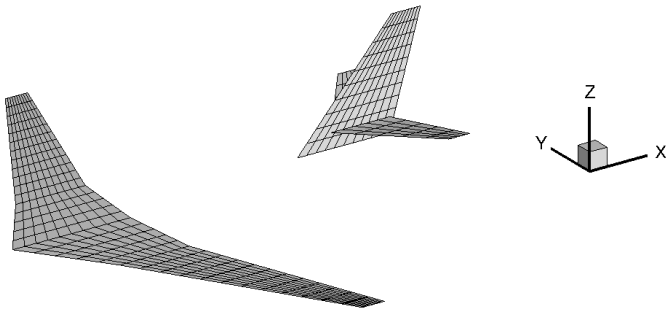

Figure 1: Doublet-Lattice grid.

Property	Wing	Horizontal Tail Plane	Vertical Tail Plane
Span (m)	57.80	18.00	11.75
Aspect ratio	8.7	4.1	1.7
Root chord (m)	13.02	6.49	10.2
Sweep angle at leading edge (deg)	35.9	47.7	41.4
Taper ratio	0.591	0.354	0.317

Table 1: Geometrical properties.

3 RESULTS

The developed ROM is applied here to a generic wing-empennage model. The Double-Lattice grid is shown in Fig. 1.

Euler results generated with a grid containing approximately $1.5 \cdot 10^5$ nodes are used as reference. The selected transonic flightpoint is Mach number 0.84 and steady angle of attack 2 (deg) and its corresponding steady pressure coefficient distribution as predicted by CFD is shown in Fig. 2.

Geometrical and mass properties together with the first natural frequencies of the structure are shown in Tables 1, 2 and 3.

Results corresponding to a vertical discrete gust of gradient $H = 350$ (ft), the longest gust as specifed by the regulations, within the linear aerodynamic region (gust amplitude 1 % of the freestream velocity) are shown in Fig. 3, 4 and 5. The full unsteady correction shows always a better agreement with the full CFD-CSM results than the quasi-steady offset correction. Integrated loads as obtained by the quasi-steady offset correction are included in order to get a fair comparison against a realistic design loads level.

Property	Value
Mass (kg)	134337
Moment of inertia I_{xx}(kg·m^2)	$1.522 \cdot 10^7$
Moment of inertia I_{yy}(kg·m^2)	$1.862 \cdot 10^7$
Moment of inertia I_{zz}(kg·m^2)	$3.342 \cdot 10^7$
Center of gravity x (m)	9.9215
Center of gravity y (m)	0
Center of gravity z (m)	0.3032

Table 2: Mass properties.

Mode	Frequency (Hz)	Configuration
7	0.74	Wing bending (symmetric)
8	1.64	Wing bending (asymmetric)
9	3.10	Wing torsion (symmetric)
10	4.11	Wing bending (asymmetric)
11	6.04	Empennage bending (asymmetric)
12	6.62	Wing torsion (symmetric)

Table 3: Vibration mode frequencies.

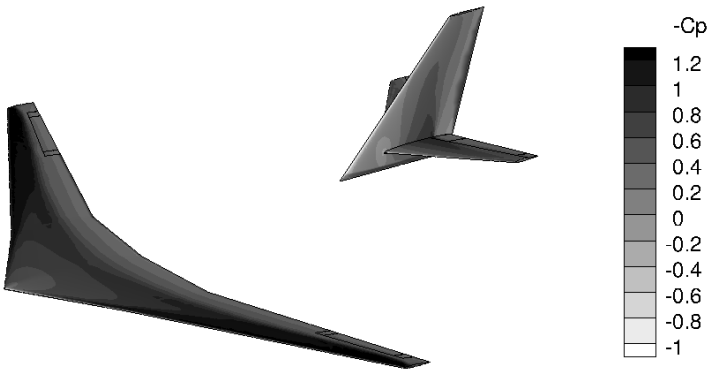

Figure 2: M=0.84, AoA=2 (deg). Euler results.

A very good agreement between the ROM and CFD-CSM values is achieved for the GAF and the aerodynamic coefficients with two correction modes (two pulse CFD computations). Additional gust lengths have been considered but are not shown here. In particular, discrete gusts with frequencies matching the second and third symmetric natural modes have been considered, obtaining also a very good agreement. As expected, the ROM prediction using only one correction mode improves with increasing gust frequency, as the nonlinearities mainly occur in the low frequency region. The bending moment distribution changes when considering the full unsteady correction, unlike for the torsional moment, which distribution is very well predicted by the quasi-steady offset correction within the linear aerodynamic region.

Results corresponding to a discrete gust of gradient $H = 350$ (ft) within the nonlinear aerodynamic region (gust amplitude 5 % of the freestream velocity) are shown in Fig. 6, 7 and 8.

Again, a very good agreement of GAF and aerodynamic coefficients with two correction modes is observed. Only small differences appear for the local pitch moment at the wing tip. The main drawback is that the correction in the nonlinear region now depends on the gust length under consideration. Unlike for the linear aerodynamic region the torsional moment distribution is not accurately predicted by the quasi-steady nor by the linear full unsteady correction. As expected, the quasi-steady correction lacks of the amplitude nonlinear effects, as an incremental angle of attack of 0.1 (deg) as defined in section 2.3.2.

4 CONCLUSION

A ROM in frequency domain has been presented. It has been shown that only two correction modes (two unsteady CFD computations and the required steady state) are required for a satisfactory aerodynamics and dynamic loads prediction. The results have been compared with direct CFD-CSM computations showing an excellent agreement.

The ROM presented not only substantially improves the aircraft response prediction but also the dynamic loads distribution.

Its properties make it suitable for further applications like wake vortex encounter. Also, a state-space system generation for closed loop applications can be developed from the generated frequency domain description.

5 REFERENCES

[1] Da Ronch, A., Tantaroudas, N. D., Timme, S., and Badcock, K. J., *Model Reduction for Linear and Nonlinear Gust Loads Analysis*, AIAA 2013-1492.

[2] Timme, S., Badcock, K. J., and Da Ronch, A., *Linear Reduced Order Modelling for Gust Response Analysis using the DLR-TAU Code*, IFASD 2013.

[3] Bartels, R., *Developing an Accurate CFD Based Gust Model for the Truss Braced Wing Aircraft*, AIAA 2013-3044.

[4] Wales, C., Gaitonde, A., and Jones, D., *Reduced Order Modeling for the Gust Response of the FFAST Wing*, IFASD 2013.

[5] Raveh, D. E., *Identification of Computational-Fluid-Dynamics Based Unsteady Aerodynamic Models for Aeroelastic Analysis*, Journal of Aircraft, Vol. 41, No. 3, 2004.

[6] Zaide, A., and Raveh, D., *Numerical Simulation and Reduced-Order Modeling of Airfoil Gust Response*, AIAA Journal, Vol. 44, No. 8, 2006.

[7] Raveh, D. E., *CFD-Based Model of Aerodynamic Gust Reponse*, Journal of Aircraft, Vol. 44, No. 3, 2007.

[8] Raveh, D., *CFD-Based Gust Response Analysis of Free Elastic Aircraft*, ASD Journal, Vol. 2, No.1, pp. 23-34, 2010.

[9] Raveh, D. E., *Aerodynamic Gust Response in High Angles of Attack*, 54th Structures, Structural Dynamics and Materials Conference, April 2013, SDM-28.

[10] Chen, P. C., Silva, R.G.A., and Liu, D.D., *Transonic AIC Weighting Method using Succesive Kernel Expansion*, AIAA 2005-1991.

[11] Thormann, R., *Correction of aerodynamic influence matrices for tranonic flow*, CEAS Aeronautical Journal, Vol. 5, pp. 435-446.

[12] Dimitrov, D., and Thormann, R., *DLM-Correction Method for Aerodynamic Gust Response Prediction*, IFASD 2013.

[13] Henderson, H. V., and Searle, S. R., *The vec-permutation matrix, the vec operator and Kronecker products: a review, Linear and Multilinear Algebra*, 1981, Vol. 9, pp. 271-288.

[14] Yang, W. Y., Cao, W., Chung, T.S., and Morris, J., *Applied numerical methods using Matlab.*

[15] Brink-Spalink, J., and Bruns, J. M., *Correction of unsteady aerodynamic influence coefficients using experimental or CFD data*, Airbus Operations GmbH, 2001.

[16] Miller, K. S., *Complex linear least squares.*

[17] Karpel, M., and Shousterman, A., *Combined frequency and time domain solutions for aeroservoelastic response with nonlinearities*, IFASD 2013.

[18] Schwamborn, D., Gerhold, T., and Henrich, R., *The DLR TAU-Code: Recent Applications in Research and Industry*, European Conference on Computational Fluid Dynamicx (ECCOMAS), Sept. 2009.

[19] Singh, R., and Baeder, J. D., *Direct Calculation of Three-Dimensional Indicial Lift Response Using Computational Fluid Dynamics*, Journal of Aircraft, Vol. 34, No. 4, 1997.

[20] Sitaraman, J., Iyengar, V. S., and Baeder, J. D., *On Field Velocity Approach and Geometric Conservation Law for Unsteady Flow Simulations*, AIAA 2003-3835.

[21] Wales, C., Jones, D., and Gaitonde, A., *Prescribed Velocity Method for Simulation of Aerofoil Gust Responses*, Journal of Aircraft, Vol. 52, No. 1, 2015.

[22] Marques, A. N., and Azevedo, J. L. F., *Numerical Calculation of Impulsive and Indicial Aerodynamic Responses Using Computational Aerodynamics Techniques*, Journal of Aircraft, Vol. 45, No. 4, 2008.

[23] Quero, D., Jenaro, G., and Krüger, W. R. *On an Innovative Approach to account for Gust Aerodynamic Nonlinearities*, AIAA 2015-0252.

[24] Gelb, A, and Vander Velde, W. E. *Multiple-Input Describing Functions and Nonlinear System Design*, McGraw-Hill.

6 COPYRIGHT STATEMENT

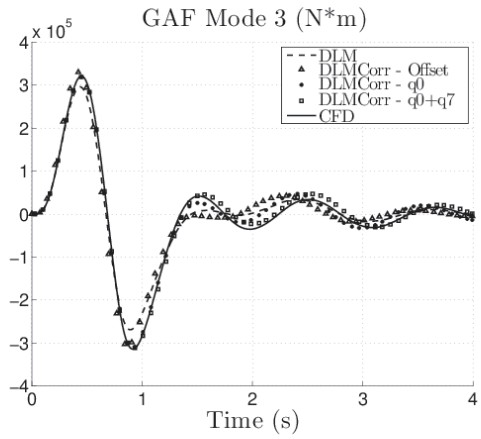

(a) Heave.

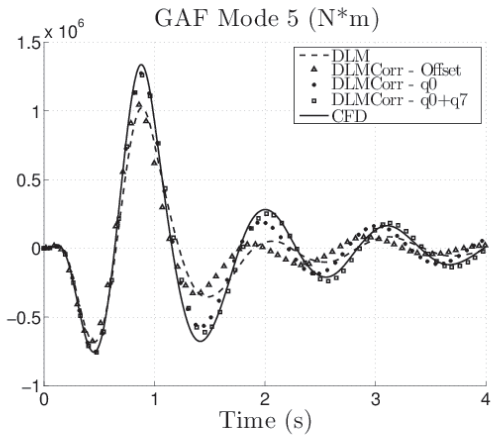

(b) Pitch.

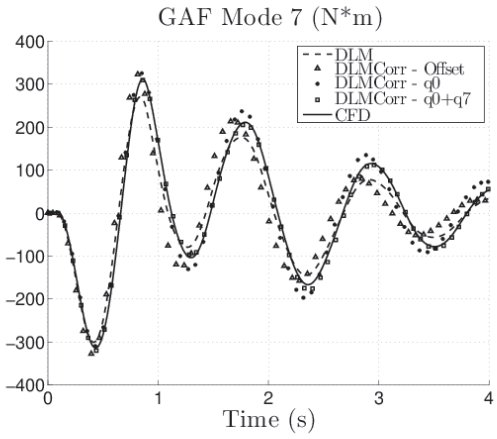

(c) First bending.

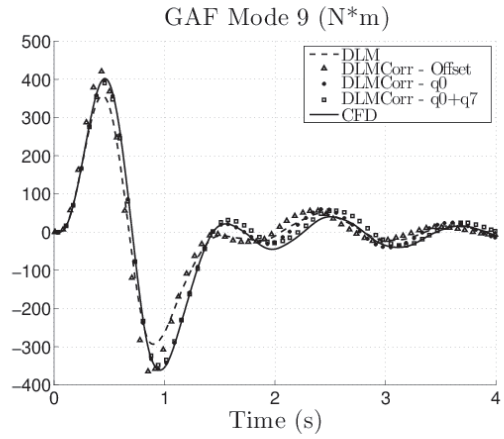

(d) Second bending.

Figure 3: M=0.84, AoA=2 (deg) in linear region. GAF.

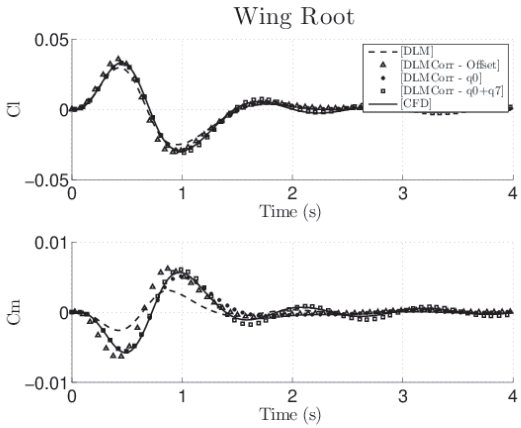

(a) Local lift and local moment at the wing root.

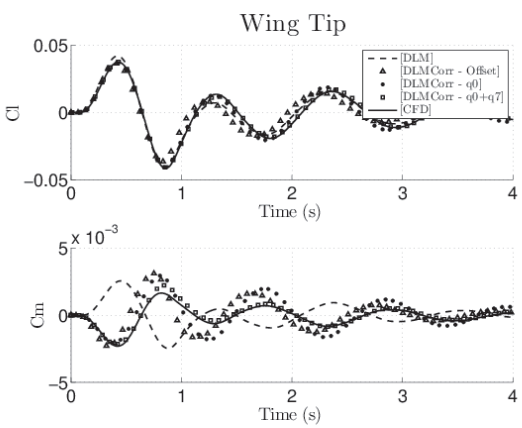

(b) Local lift and local moment at the wing tip.

Figure 4: M=0.84, AoA=2 (deg) in linear region. Local aerodynamic coefficients.

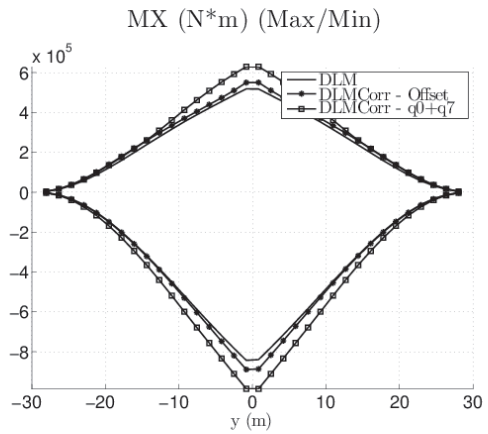

(a) Bending moment.

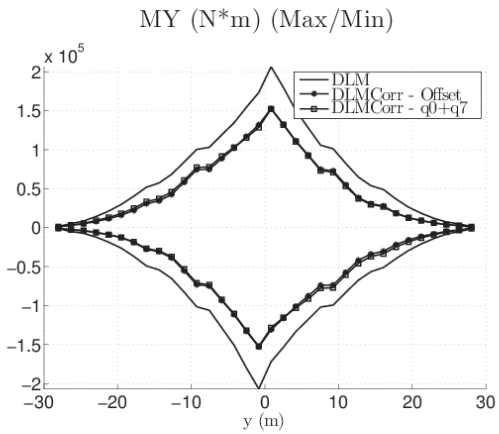

(b) Torsional moment.

Figure 5: M=0.84, AoA=2 (deg) in linear region. Wing integrated loads envelope.

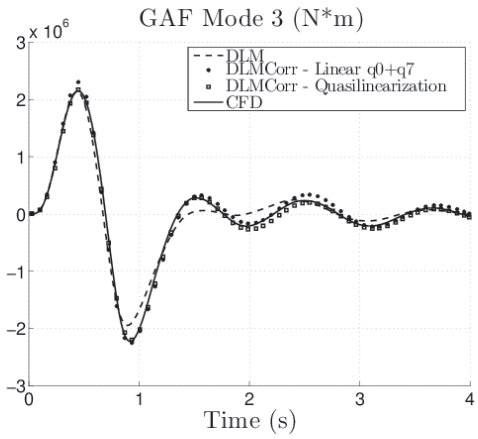

(a) Heave.

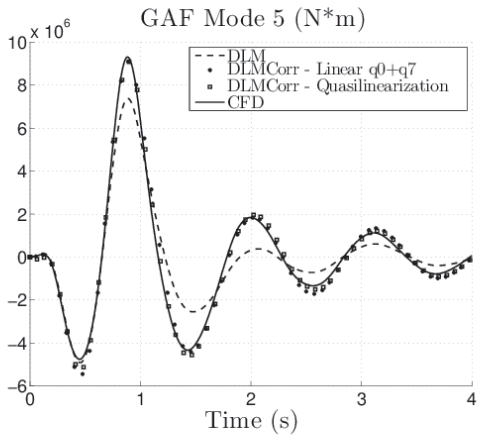

(b) Pitch.

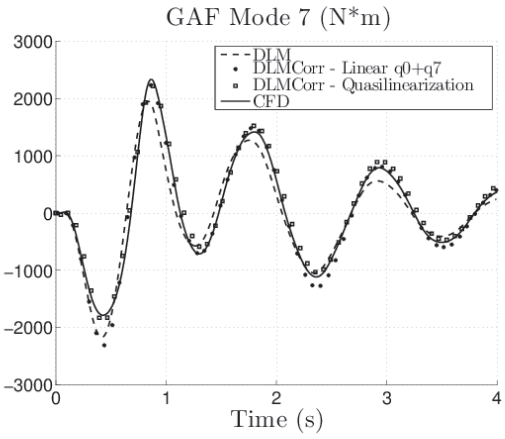

(c) First bending.

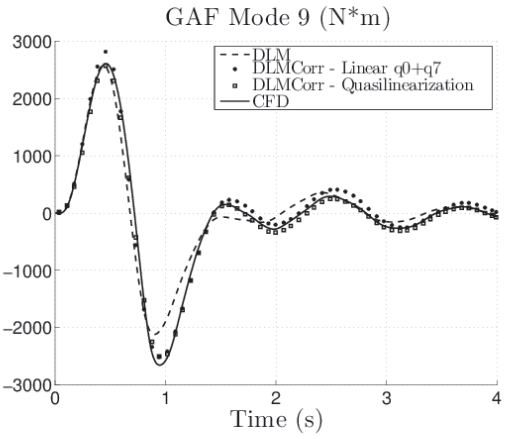

(d) Second bending.

Figure 6: M=0.84, AoA=2 (deg) in nonlinear region. GAF.

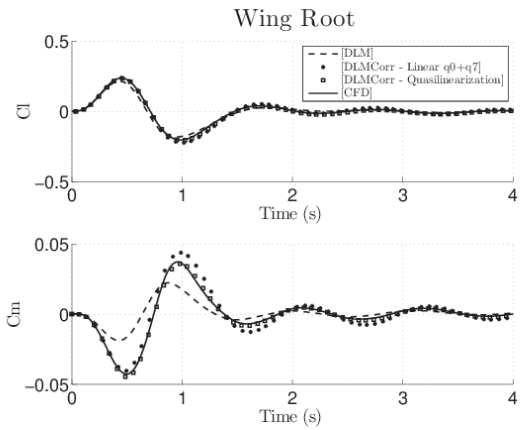

(a) Local lift and local moment at the wing root.

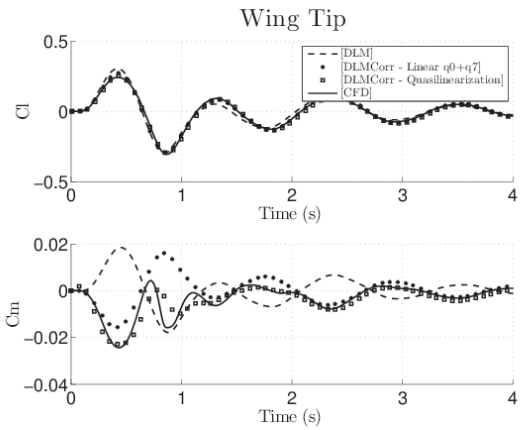

(b) Local lift and local moment at the wing tip.

Figure 7: M=0.84, AoA=2 (deg) in nonlinear region. Local aerodynamic coefficients.

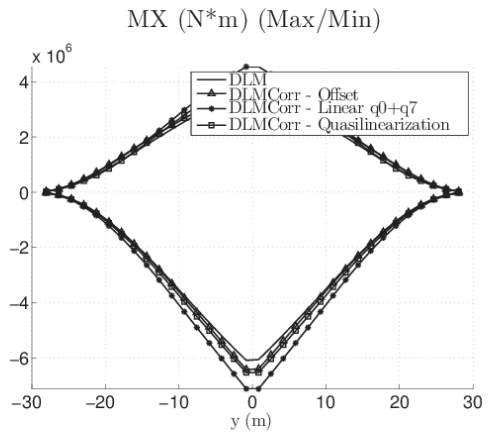

(a) Bending moment.

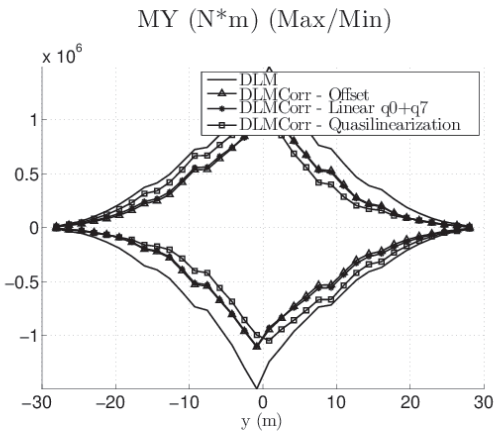

(b) Torsional moment.

Figure 8: M=0.84, AoA=2 (deg) in nonlinear region. Wing integrated loads envelope.